Journal of Multiscale Modeling, Volume 12, Issue 1, March 2021, Article number 2050009
DOI: 10.1142/S1756973720500092

Prediction of reheat cracking behaviour in a service exposed 316H steam header

Haoliang Zhou[1], Ali Mehmanparast[2], Kamran Nikbin[1]

[1]Department of Mechanical Engineering, Imperial College London, South Kensington Campus, London, SW7 2AZ, UK

[2]Offshore Renewable Energy Engineering Centre, Cranfield University, Cranfield, Bedfordshire, MK43 0AL, UK

Abstract:

Reheat cracking in an ex-service Type 316H stainless steel steam header component has been investigated in this study. The examined steam header was in service for 87,790 hours and the cracks in this component were found in the vicinity of the weld toe. The root cause of this type of failure was due to the welding residual stresses. The welding-induced residual stresses had been present in the header at the early stage of the operation and were released during service. In this paper a novel technique has been proposed to simulate the residual stress distribution normal to the crack direction by applying remote fixed displacement boundary conditions in an axisymmetric model. This approach can simulate the presence of residual stresses in actual components without the need to develop full weld simulation to quantify them. The predicted residual stress levels and distributions normal to the crack direction have been found in good agreement with the measured residual stresses available in the literature for a similar header. The creep crack growth (CCG) rates have been characterised using the fracture mechanics C^* parameter and estimated using predictive models.

Keywords: Reheat cracking; Residual stresses; Creep Crack Growth (CCG); 316H; C^* correlation

Nomenclature:

θ	Angular position	ε	Strain
ε^c	Creep strain	ε^e	Elastic strain
ε^p	Plastic strain	ε_f	Creep Ductility
ε_f^*	Equivalent creep ductility	ε^t	Total strain
$\dot{\varepsilon}_A^c$	Average creep strain rate	$\dot{\varepsilon}_{ref}^c$	Reference creep strain rate
$\dot{\varepsilon}_s^c$	Steady state creep strain rate	σ_e	Equivalent stress

σ_{ij}	Stress tensor	σ_{ref}	Reference stress
σ_y	Yield stress	v	Poisson's ratio
a	Crack length	A_A	Norton power-law constant under average creep stage
A_s	Norton power-law constant under secondary stage	C^*_{ref}	Reference stress estimate of C^*
E	Young's modulus	K	Stress intensity factor
n	Creep stress exponent	n_A	Average creep stress exponent
n_s	Steady state creep stress exponent	P	Load
P_{LC}	Limit load	t_r	Time to creep rupture
BC	Boundary Condition	BM	Base Metal
C(T)	Compact Tension specimen	CCG	Creep Crack Growth
DCT	Displacement-controlled tension	DH	Deep Hole drilling
LCT	Load-controlled tension	MMA	Multi-pass Manual Metal Arc
HAZ	Heat Affected Zone	FE	Finite Element
Pσ	Plane stress	Pε	Plane strain
WM	Weld metal	RS	Residual Stress

1. Introduction

Reheat cracks have been found in five, out of seven, of EDF Energy's advanced gas cooled reactors (AGRs) operating at elevated temperature in the range of 500-650°C in excess of 10^5 h [1], [2]. The reheat cracking mechanism has been systematically studied in Type 316H stainless steel headers and it has been found that the existence of welding residual stresses can accelerate the accumulation of creep damage [1]–[12]. In this material, the triaxial state of residual stresses could not entirely be relieved after welding. The distribution of existing residual stress depends on many factors, including material properties, component structures, constraint conditions, heat input, number of weld passes and welding sequence [13]. Therefore, to simulate the welding residual stress in Finite Element (FE) simulations, the effects of section thickness, temperature-based material properties and state of as-welded stress triaxiality are required to be considered, which result in a difficult and time-consuming analysis [2]. The reason for reheat cracks is mainly due to the creep dominated relaxation of the highly triaxial residual stresses induced by welding processes. The main aim of this study is to develop a simplified FE method to predict residual stress re-distributions subsequent to creep crack growth (CCG).

In the simplified FE technique proposed in this study, the residual stresses in a steam header component have been predicted using an axisymmetric numerical model, by introducing a remote load generated from a fixed displacement. The displacement controlled internal tensile stress was relaxed in the model, the decrease in load of the header component held at the fixed displacement,

corresponding with creep crack initiation and propagation which occur at the location that has the highest stress and the weakest bond at high temperature. For comparison purposes, FE analysis was performed on a case similar to that of previously described in [3], [8], [9], [14], [15] and the measured and predicted residual stresses for the header component have been compared to those of available in the literature.

According to the prediction models developed by Nikbin-Smith-Webster (NSW), the creep crack growth behaviour of the material can be predicted using the fracture mechanics parameter C^* and uniaxial creep ductility [16], [17]. The approximate NSW (NSWA) model which is a simplified version of the original NSW model, has been applied in this study since it has been proved to be a suitable prediction model for the material examined in this study [18].

2. Steam Header Service Condition

Type 316H stainless steel welded nozzle and steam header component was provided by EDF Energy, taken from a power plant in the UK. A nozzle was attached to the steam header using manual metal arc welding [9]. After welding, the processes of 3-hour heat treatment at 1050 °C and subsequent water quench were applied. The component was taken out of service after 87,790 hours of operation at 525 °C, since some cracks were detected in the component which had been propagated with a length of around 8-15 mm. Figure 1 shows the steam header from which the region of interest (see the circled area) was removed to study the cracking behaviour with respect to the welding location. A cross section of the extracted region showing the nozzle/header branch is shown in Figure 2, where the main dimensions were used in FE model. A primary reheat crack is observed in Figure 2 and the cracking region is magnified in Figure 3. The circumferential cracks were initiated at the radius from the nozzle near the weld toe and grown normal to the corner of the joint of header and nozzle, away from the weld. The crack in Figure 3 is 12 mm long with a deviation angle of $\theta = -132.5^{\circ}$ from the horizontal axis.

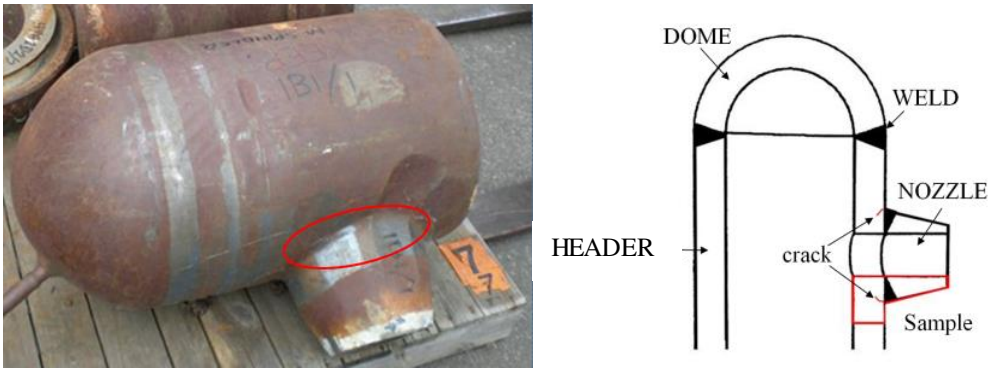

Figure 1: (a) Illustration and (b) schematic of the steam header, identifying the welding and cracking location

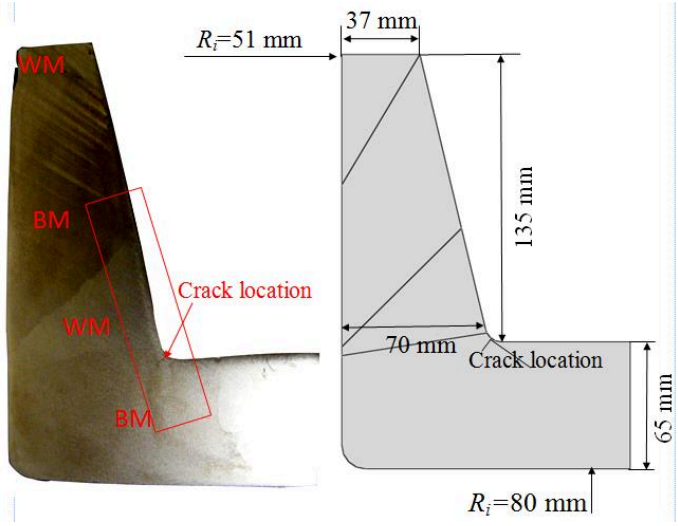

Figure 2: A cross section of the nozzle/header joint, showing the main dimensions used in the FE model and the positions of the crack, base and weld metal

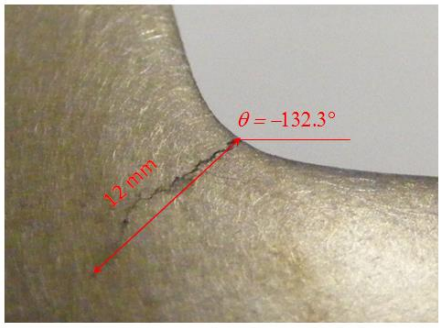

Figure 3: Magnified cracking region

Due to the lack of residual stress measurement data on the examined steam header the predicted FE results were compared with a different but similar header component. The archetypal austenitic header, which was investigated by Smith et al. and Hayhurst [3], [8], [9], [14], [15], was also taken from the same power station, serviced at 525 °C. The main geometrical dimensions, weld position, crack position, which is shown in Figure 4, are also similar to the studied component. Thus, the resultant residual stress approximations from these two components are assumed to be equivalent and comparable.

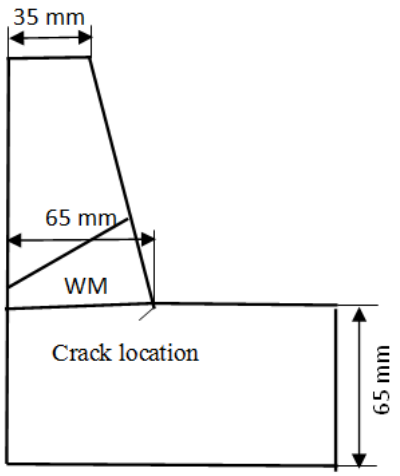

Figure 4: The main dimensions, weld metal and crack positions in a comparable welded component [14]

According to Ref [14], the stress normal to the crack face was measured using the Deep Hole Drilling (DH) method and predicted using FE welding simulations . Residual stress distributions have been measured prior-to-service (as-welded) and ex-service after 55,000 hours of exposure at 525°C. The results of pre and post-measured and simulated residual stress normal to the crack face are shown in Figure 5.

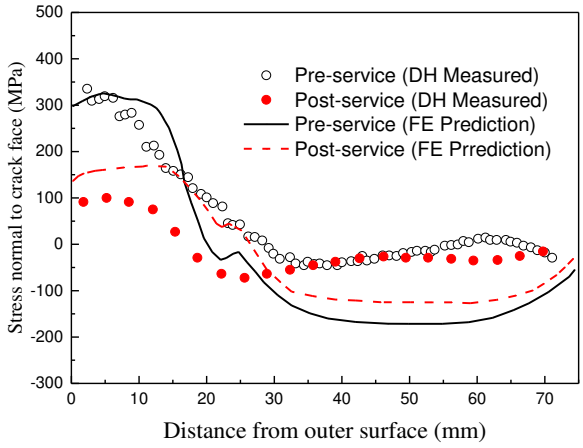

Figure 5: Measured and predicted stress along the crack growth direction [14]

3. Creep Deformation and Crack Growth

3.1 Mechanical and Creep Properties

The total strain, ε^t in high temperature comprises of a time dependent creep strain ε^c component and a time independent strain component, which can be subdivided into elastic ε^e and plastic component ε^p, defined as

$$\varepsilon^t = \varepsilon^e + \varepsilon^p + \varepsilon^c \quad (1)$$

True elastic-plastic properties of the base metal (BM) and weld material (WM) obtained from tensile tests measured using the digital image correlation (DIC) technique have been reported in Ref [19] and shown in Figure 6. The material properties were employed in elastic-plastic FE analyses. The elastic Young's modulus and yield stress (0.2% proof stress) are provided in Table 1.

The steady state secondary creep strain rate, $\dot{\varepsilon}_S$ may be related to the equivalent stress, σ_e, using a power-law relationship

$$\dot{\varepsilon}_S = A_s \sigma_e^{n_s} \quad (2)$$

where σ_e is equivalent stress, A_s and n_s are the steady state power-law constants.

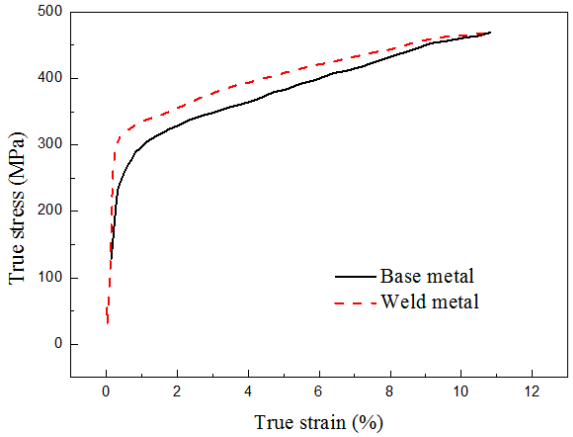

Figure 6: Tensile response from DIC measurement in base metal and weld metal at high temperature based on true stress and strain definitions

Table 1: A summary of material properties

	Young's modulus, E(GPa)	Poisson's ratio, ν	Yield stress σ_y (MPa)	A_s ($h^{-1}MPa^{-n}$)	n_s	A_A ($h^{-1}MPa^{-n}$)	n_A
Base metal	140	0.3	275	3.96×10^{-32}	10.9	9.82×10^{-40}	14.0
Weld metal	155	0.3	185	2.68×10^{-32}	10.9	1.0×10^{-39}	14.0

The effect of all three creep stages is usually described by the average creep strain rate which can be defined as the ratio of the creep ductility ε_f to the time to rupture t_r. The average creep strain rate, $\dot{\varepsilon}_A$, is always greater than the steady creep strain rate $\dot{\varepsilon}_S$. Similar to the behaviour of $\dot{\varepsilon}_S$, $\dot{\varepsilon}_A$ can also be expressed as a power-law form as

$$\dot{\varepsilon}_A^c = A_A \sigma_e^{n_A} = \frac{\varepsilon_f}{t_r} \tag{3}$$

where A_A and n_A are material constants which can be obtained from rupture data.

The uniaxial creep rupture tests were performed on the base and weld metal of Type 316H stainless at 550°C. The results are reported in Ref [12]. The key creep properties are given in Table 1. The average creep strain rate, $\dot{\varepsilon}_A^c$, was mainly used for stress and damage analysis. Also note that the stress distributions obtained from the $\dot{\varepsilon}_A^c$ was compared to the secondary creep strain rate, $\dot{\varepsilon}_s^c$.

3.2 NSWA Creep Crack Growth Prediction Model

In order to predict creep crack growth behaviour, the creep crack growth rate, $\dot{a}$, should be determined and correlated with an appropriate fracture mechanics parameter. If the crack growth rate is modelled successfully, it can be used to assess the life of a serviced component that cannot be simulated from laboratory test data. When creep deformation predominates the stress distribution, the steady state crack growth rate, $\dot{a}$, is commonly characterized by C^*.

For steady state creep, the evaluation of C^* might be obtained by finite element analysis for materials with creep rates defined by a secondary creep law with a simple power dependence on stress. In practice, as suggested in R5 [20], reference stress approach is recommended to calculate C^* to estimate the risk for creep rupture and it usually provides a conservative bound. The definition of C^* using reference stress is given by

$$C^*_{ref} = \dot{\varepsilon}^c_{ref} \sigma_{ref} \left(\frac{K(a)}{\sigma_{ref}} \right)^2 \tag{4}$$

where K is the stress intensity factor which is a function of crack length a, σ_{ref} is reference stress, $\dot{\varepsilon}^c_{ref}$ is the reference creep strain rate which can be obtained by Norton's law, described by

$$\dot{\varepsilon}^c_{ref} = A_A \sigma_{ref}^{n_A} \tag{5}$$

The reference stress is defined by

$$\sigma_{ref} = \sigma_y \frac{P}{P_{LC}} \tag{6}$$

where P is load, P_{LC} is the limit load which describes a maximum sustainable load for elastic-perfectly plastic materials and is often used to determine the extent of plasticity in structures. Knowledge of limit load can aids designing mechanical properties of components and structures, since limit load provides information of the modes of failure associated with load-controlled effects [21] [22]. P_{LC} in Eq.**(6)** is the function of normalised crack size and is related to the yield stress, σ_y whilst σ_{ref} is independent of σ_y .

The creep crack growth rate can be predicted by NSWA model, in the form of

$$\dot{a}_{NSWA} = \frac{3C^{*0.85}}{\varepsilon_f^*} \tag{7}$$

where $\dot{a}_{NSWA}$ is the creep crack growth rate calculated by NSWA model, the unit of $\dot{a}_{NSWA}$ is in [mm/h] and C^* is in [MPam/h]. Under steady state conditions, the CCG rate is mainly dependent on multiaxial creep ductility ε_f^* .

As discussed in Ref [21][22][23][24], from the long/short term data, the failure ductility for 316H stainless steel at around 550 °C could be simplified to an approximate lower/upper shelf, with a transition region in between, the results can be seen in Figure 7 [21]. The lower shelf is around 0.9%, which occurs at long term, low stress condition. Uniaxial creep ductility of $\varepsilon_f = 0.9\%$ is used in this study. Here ε_f^* is taken as the equivalent uniaxial failure strain, which is ε_f for plane stress condition and ε_f / 30 for plane strain condition.

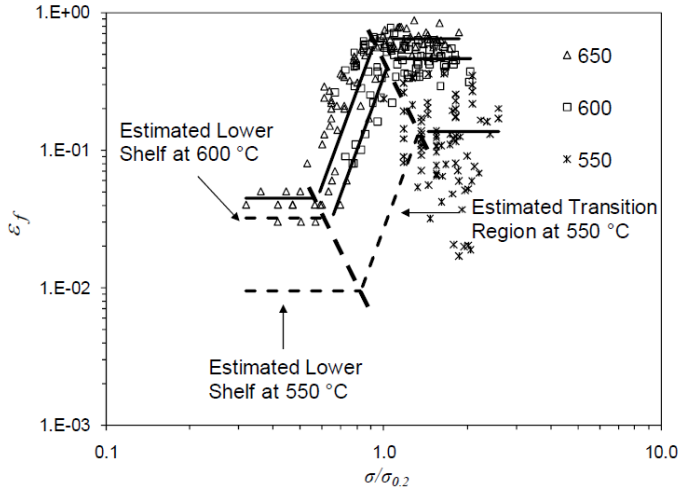

Figure 7: Creep ductility profiles in a range of stresses and temperatures [22]

4. Finite Element Simulations

4.1 Mesh and Step Design in Finite Element Analysis

Figure 8 (a) shows a two-dimensional axisymmetric FE model designed in ABAQUS software package. The heat affected zone (HAZ) was not considered due to the complexity in defining its mechanical and creep properties, thus a bi-material model was employed in simulations. As shown in Figure 8 (b), the mesh design had elements of 100 µm ×100 µm at the crack initiation region which were coarsened away from the cracking region. The full model includes 12,248 quadrilateral-dominated elements.

Having obtained the elastic-plastic solution by applying a load in the first step, the component was allowed to creep at 550°C in the second step. Stress analysis was performed between the simulation time of $t = 0$ and $t = 55{,}000$ hours.

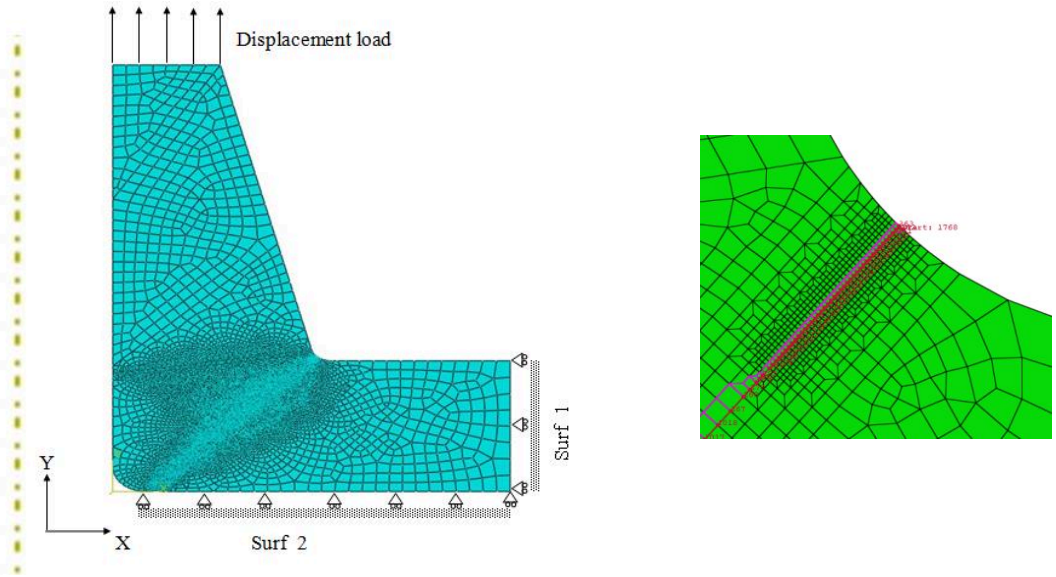

(a) (b)

Figure 8: (a) The modelled geometry in FE after meshing, (b) Details of the mesh detain near the crack growth region.

4.2 User-defined Subroutine

A user-defined subroutine allowed the recording of the stress normal to the crack face, $\sigma_{\perp}$. The calculation of $\sigma_{\perp}$ in a 2D model is according to stress coordinate transformation equation as follows

$$\sigma_{\perp} = \frac{\sigma_{11} + \sigma_{22}}{2} - \frac{\sigma_{11} - \sigma_{22}}{2}\cos 2\theta - \sigma_{12}\sin 2\theta \qquad (8)$$

where σ_{11}, σ_{22} are the principal stress in the x and y direction, σ_{12} is shear stress, $\theta = -132.5^{\circ}$.

4.3 Loading Conditions

As indicated in Figure 1-Figure 3, reheating cracks grew at an angle from the outer to inner surface of the header due to the existence of welding residual stresses. The residual stress acting on the nozzle which leads to crack initiation and crack propagation was modelled in the form of tensile stresses. The ABAQUS analysis allowed both load-controlled (LCT) and displacement-controlled (DCT) tension. The load controlled method was used to introduce a direct load on the component whilst the displacement controlled test was used to apply a displacement on a body. In the LCT, the tension surface was constrained to a reference node which could avoid any stress concentration on the loading position. The two tensile conditions are examined in the current study. Also, in order to obtain a comparable level of stress distribution to the measured data, a sensitivity study was made for the stresses around the nozzle. All the possible load conditions are shown in Table 2.

Table 2: Possible load conditions

Model ID	Load Type	Load	Boundary condition
LC-LCT1	Load-controlled tension	1300 KN	U2=0 on surf1
LC-DCT1	Displacement-controlled tension	0.25mm	U2=0 on surf1
LC-DCT2	Displacement-controlled tension	0.5mm	U2=0 on surf1
LC-DCT3	Displacement-controlled tension	1.0mm	U2=0 on surf1
LC-DCT4	Displacement-controlled tension	2.0mm	U2=0 on surf1

4.4 Boundary Conditions

A sensitivity study of boundary condition is performed on the nozzle/header component. Under axisymmetric condition, the inner side of nozzle has been fixed. Therefore, the boundary condition can be placed on surf 1 or surf 2 or combination of two, as shown in Figure 8.

It has been found that when y-direction (U2) is fixed there is no need to consider the combination of two surfaces, 2D rotation condition (UR3) and x-direction (U1) on surf 2. Thus, possible boundary conditions are limited to three cases, which is shown in Table 3. The predicted stress along the crack path in different boundary conditions was compared with the measured data.

Table 3: Possible boundary conditions

Model ID	Displacement Controlled Load	U1-surface 1	U2-surface 1	U1-surface 2
BC-1	0.5 mm	-	Fixed	-
BC-2	0.5 mm	Fixed	Fixed	-
BC-3	0.5 mm	-	-	Fixed

4.5 Mesh and Step Design for *C** Analysis

According to Eq **(4)**, current measurement of *C** based on the reference stress requires obtaining the stress intensity factor, *K* and the reference stress, σ_{ref} in different crack length. Firstly, 2D linear elastic analysis was performed to determine *K* with crack length ranging from 5 to 30 mm. The elements at the crack tip were designed with collapsed type and expanded to the type of sweep away from crack-tip region. Figure 9 illustrates the localised mesh design considering a 10mm initial crack at an angle of θ = -132.5° from the horizontal axis, the elements at the crack tip are magnified. After positioning the crack tip and its direction during the first step, *K* can be obtained from linear elastic FE analysis. Secondly, the reference stress needs to be calculated. The current study allowed a displacement controlled tension load to be applied in the model with the same mesh design showing in Figure 9. The model had homogeneous and elastic-perfectly plastic material properties. As load increased, the elements at the crack tip were firstly collapsed. Following that, sufficiently large distortion occurred. The nodal force on the corresponding elements would increase firstly and remain constant. The constant force was considered as the limit load. After reaching the limit load, FE model would collapse. The reference stress was therefore calculated based on Eq. (6). Subsequently the reference strain was obtained using Eq. (5) and finally *C** was calculated according to Eq. (4).

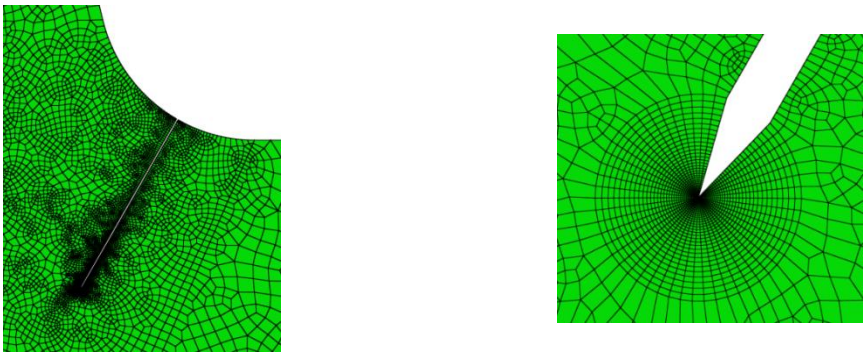

Figure 9: (a) FE mesh design to determine stress intensity parameter with a 10mm crack, (b) showing the magnified crack tip area

5. Results and Discussion

5.1 Residual Stress Predictions

The predicted residual stresses were expected to have similar trends compared to the residual stress distribution benchmark shown in Figure 5. Therefore, sensitivity studies were applied to identify the optimum loading profile and boundary conditions in the current model that would best represent the actual measured residual stress data that was available for the similar header reported in Ref [4, 9, 11, 14]. According to Table 2, load-controlled tension (LCT) and displacement-controlled tension (DCT) were employed in the current non-linear analysis. It has been found that stress in all directions (s11, s22, s12 and von-Mises stress) had the same distributions when compared with displacement of 0.25mm (LC-DCT1) and load of 1300 KN (LC-LCT1).

Despite the same distribution in the loading procedure, displacement controlled analysis was preferable for the following long term stress relaxation condition. During the stress relaxation, the examined header component would begin to demonstrate strain-softening behaviour and a gradual decrease in load carrying capacity with increasing strain. The release of the strain energy could result in a formation of a crack which may occur at the location that has the highest stress and the weakest bond. Under the fixed displacement, the crack would continue to develop to release more energy. However, in the fixed load, the crack may result in sudden failure due to the input of external energy. Knowing this, a sensitivity analysis was conducted for the stresses acting along a direction perpendicular to the nozzle's surface with different vertical displacements ranging from 0.25mm to 2.0 mm, in order to compare with the stress distributions from the measured data. The stress normal to the crack face was considered and the results are shown in Figure 10.

All predicted stress distributions shown in Figure 10 demonstrate a tensile residual stress close to the steam header's outer region while compressive stresses can be observed near the inner regions. Among them, the LC-DCT2 simulation with 0.5 mm displacement had a peak tensile value of 292 MPa, which was close to the measured data of 300 MPa. Also, the stress distribution was at a comparable level to the measured data. Therefore, LC-DCT2 acceptably represents the residual stress profile in terms of stress normal to the cracking direction in the header.

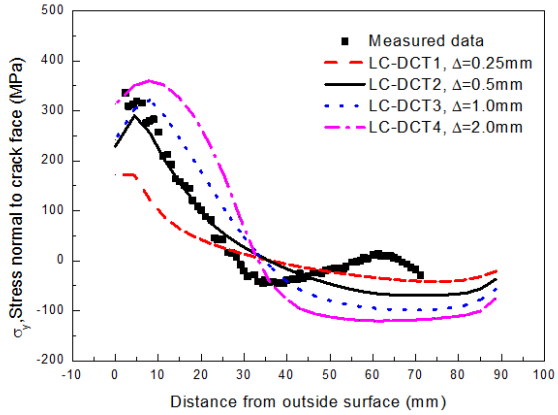

Figure 10: Predicted data under different vertical displacements compared with measured stress distributions along the crack direction in pre-service condition

As mentioned in Table 3, three cases of boundary conditions were considered. The predicted stress along the crack path in the three cases with different boundary conditions was compared with the measured and simulated data published in Ref [14]. The results are shown in Figure 11 (a) for pre-service and (b) for 55,000 hours post-service. The average strain rate $\dot{\varepsilon}_A^c$ was applied in these FE simulations.

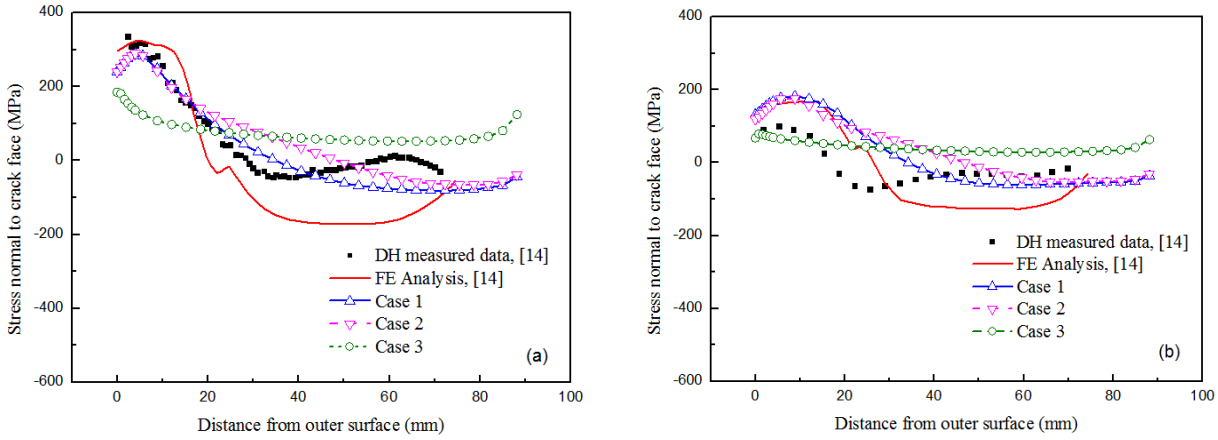

Figure 11: Comparison of the measured and predicted stresses for (a) pre-service and (b) after service

In Figure 11 (a), the initial stress distributions on the pre-service condition were similar to the measured data, since the maximum tensile stress occurred at the outer surface, which is a geometric stress concentration area, and then decreased to compressive levels along the crack direction. The stress profile in Case 1 was in better agreement to the measured data, among the three cases and the FE predictions in Ref [14]. In Figure 11 (b), after a 55,000 hour creep, the residual stress was overestimated compared to the measured data. Stress relaxation rate in Case 1, for instance, was 36%, which was lower than a 75% relaxation in the measured data. This difference may be due to the micro-structural changes near the welding region, the existence of plastic strain in the component post-fabrication and the higher creep strain rate than the base metal value employed [2], [25] [26].

Contour plots of the stress profiles on the pre and post-service are shown in Figure 12-Figure 14, for the three cases examined. In Figure 12, it can be observed that a tensile residual stress close to the steam header's outer region, while a compressive stress was within the inner region. In Figure 12(a), the peak value of stress was 292 MPa in tensile and 186 MPa in compressive form. The maximum tensile value was fairly similar to the measured crack initiation stress. After 55,000 hours as shown in Figure 12(b), the peak tensile and compressive stress had a partial relaxation of 36% in magnitude. It is worth noting that the tensile region during relaxation appears to move inside and follows the expected crack path. Therefore, the crack initiation would occur in the area which has the highest tensile stress and the stresses would redistribute as the crack propagates.

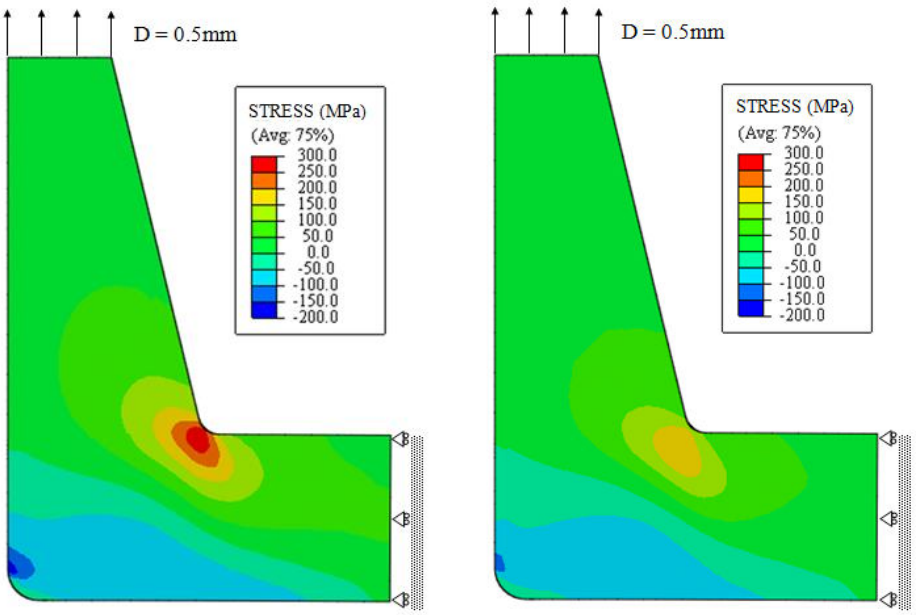

(a) *(b)*

Figure 12: Case 1-Stress distribution perpendicular to the crack plane for (a) pre-service (b) after service

In Case 2, the stress distribution shown in Figure 13 is similar to those observed in Figure 12, except a source of large tensile stresses at the fixed surface, due to the additional boundary condition. This stress distribution would possibly influence the stress redistribution along the crack path.

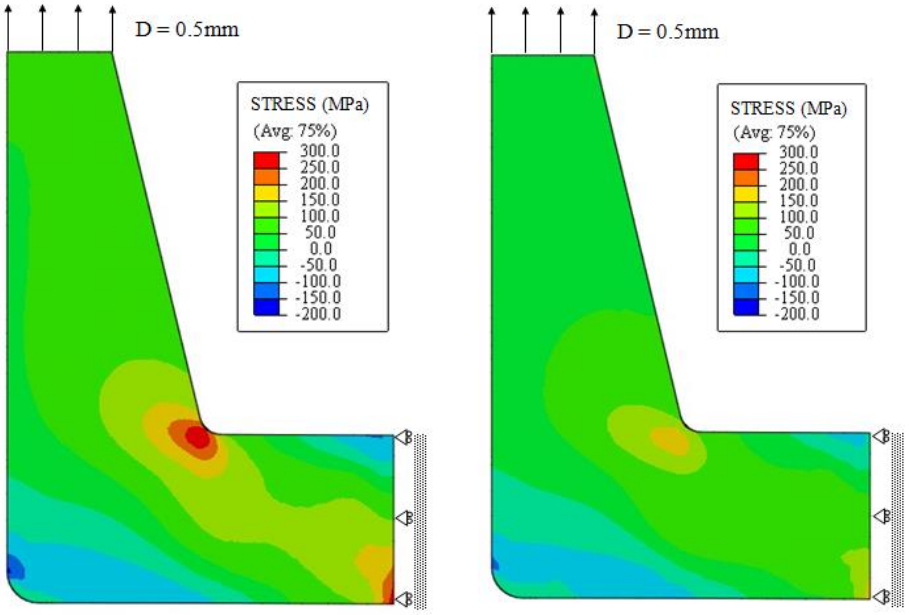

(a) *(b)*

Figure 13: Case 2-Stress distribution perpendicular to the crack face for (a) pre-service (b) after service

In Case 3, the maximum pre-serviced stress along the crack path was 187 MPa, which is which is not enough to initiate the crack.

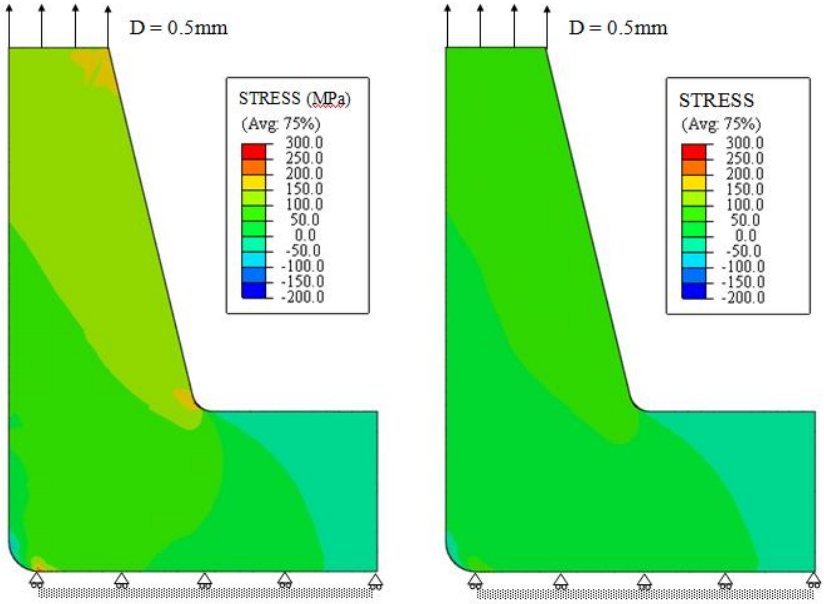

(a) *(b)*

Figure 14: Case 3-Stress distribution perpendicular to the crack face for (a) pre-service (b) after service

The stress distribution after relaxation was also examined for Case 1 using the steady state creep strain rate data shown in Table 1. The maximum tensile stress after a steady state creep was 220MPa, larger than 185MPa in average strain rate. This extra stress relaxation might appear at towards the rupture time.

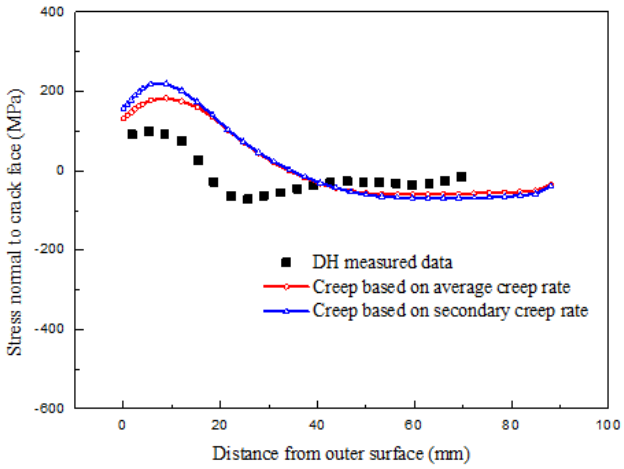

Figure 15: Stress distribution perpendicualr to the crack face after 55,000 hours using either steady state or average creep strain rate

Note that in this work the load and boundary conditions have been simplified to provide the best residual stress predictions prior to and after service, compared to available experimental measurements. Good agreements were observed between the residual stress predictions and available measurements for the header prior to component operation and after 55,000 hours of creep deformation and stress relaxation. The predicted stress normal to the crack face profile implies that the reheat cracks were initiated at a geometric stress concentration area which has highest stress, and propagate in the direction of the highest principal stress. These findings are consistent with experimental reheat cracking observations made in actual components.

5.2 Creep Crack Growth Analysis

The analysis of creep damage and the correlation of creep crack growth CCG rate has been performed in this study. There are two methods to predict creep crack growth rate, the fracture mechanics method and continuum damage model. In the current study, fracture mechanics method was considered to examine the approximate crack growth rate using NSWA model, this simplified model can reduce the testing procedure and the number of tests required to describe the material properties.

Fracture mechanics analysis assumes the presence of a crack of finite size in a component and then evaluates its propagation due to creep to determine the remaining life of the components [27]. Analysis of the model with different creep ductilities and crack lengths would result in a series of values of K and C^*. It is suggested in ASTM E 1457 [28] that K is applicable for creep-brittle materials while C^* is suitable for charactering CCG behaviour in creep-ductile materials. Type 316H is considered as a creep ductile material [29] [30] [31], thus the fracture mechanics parameter, C^*, is more appropriate and it should be matched against corresponding values for crack growth rate, $\dot{a}$, with a consideration of the validity checks.

For the widespread creep conditions NSWA model can be used to estimate the creep crack growth behaviour of the material. The use of NSWA model generally gives conservative predictions of crack propagation rate [21]. As mentioned, the basic parameters required for using the approximate methods are the elastic stress intensity factor, K, and the reference stress, σ_{ref}, as shown in Eq (4).

From the linear elastic model, the results of stress intensity factor *vs.* crack length under a displacement controlled tension analysis are plotted in Figure 16. In the elastic-linear plastic model, the FE analysis allows obtaining the value of P_{LC} / P from which σ_{ref} was calculated according to Eq **(6)**. The relationship between crack length and σ_{ref} is plotted in Figure 17 in which a

decreasing trend can be observed in the displacement controlled analysis. Using the simulations, σ_{ref} and C^{*}_{ref} values were predicted at different crack lengths, which are shown in Figure 18.

As shown in Figure 18, the NSWA prediction model provides an upper and lower bound CCG trends for the creep ductile materials under plane strain and plane stress conditions, respectively. The range between plane strain and plane stress describes the effect of constraint on crack growth due to material properties and geometric factors.

Included in Figure 18 are experimental test data in black cross from 316H stainless steel C(T) specimens of difference size. Generally, the experiential C(T) specimens were under creeping time less than 2000h at relatively high stress level, while the header component was serviced at low stresses. Dean and Gladwin [32] investigated the creep crack growth behaviour of Type 316H stainless steel C(T) specimens from low stress to high stress with the creeping time ranging from 170-16,630 hours, and they found that it is possible to reliably predict the CCG data for all tests. This validation provides a basis to compare the laboratory specimens and actual component under different loading conditions.

The two estimated lines sufficiently bound the valid data points, indicating the possibility to discuss the CCG rate under different geometry and service conditions. The lower shelf trend under plane stress condition sufficiently bound the data band, indicating a good agreement between the experimental data and predictions, while the upper shelf under plane strain condition is conservative with an over-prediction of the crack growth rate.

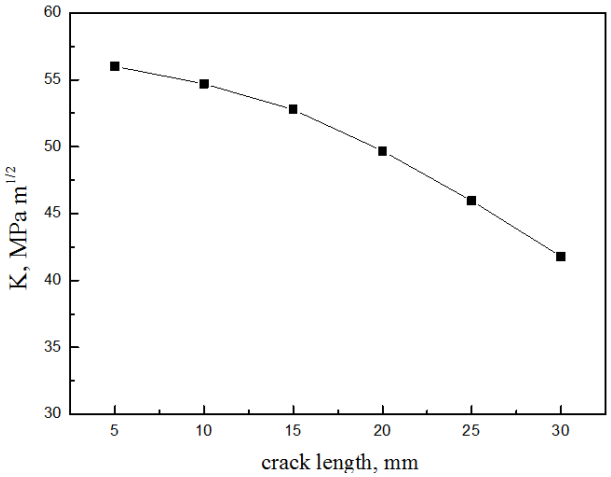

Figure 16：Stress intensity factor *vs.* crack length using displacement controlled analysis

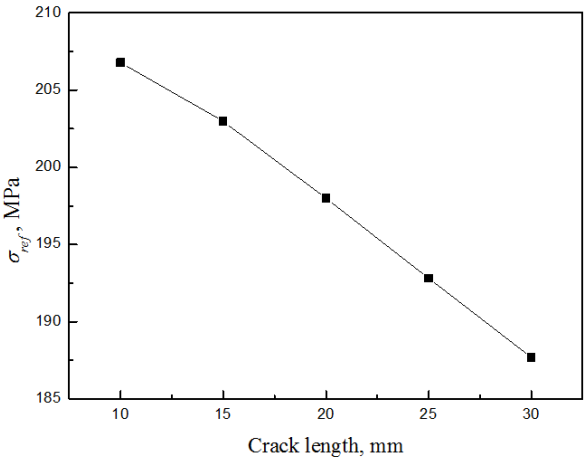

Figure 17: Reference stress σ_{ref} against creep crack length using displacement controlled analysis

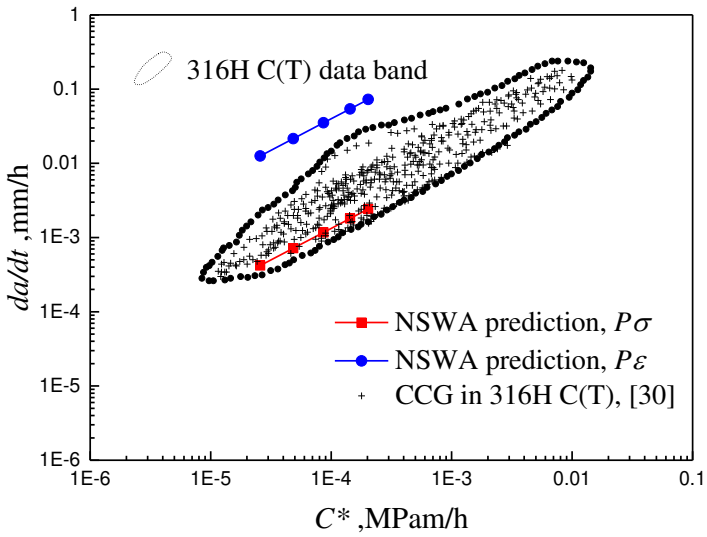

Figure 18: Creep crack growth rate predicted by NSWA equation for plane stress and plane strain condition, compared with CCG data measured in 316H C(T) specimens taken from [33]

6. Conclusion

In this paper reheat craking in an ex-service 316H welded steam header was investigated. Reheat cracks have been found in the vicinity of the weld connect to the outlet nozzle. The root cause of this type of failure was due to welding residual stress, however, detailed material properties and state of as-welded stress triaxiality are needed for an accurate prediction of welding residual stresses. A simplified method has been proposed to simulate the welding residual stress distribution in the steam header. The residual stress relaxation due to service exposure has been successfully modelled using FE simulations. Acceptable predictions were made for the stress distribution profile, possible crack location and orientation of reheat cracking. The fracture

mechanics method using the reference stress based estimate of C^* has been applied to calculate the creep crack growth rate based on the approximate NSW model. The CCG rate predictions made using this method have been found in relatively good agreement with the existing experimental data obtained from C(T) specimens tested at 550°C.

7. Reference

[1] R. A. W. Bradford, "Finite Element Modelling of Reheat Cracking Initiation in Austenitic Weldments," in *International Conference on "Assuring It's Safe,"* 1998, pp. 287–295.

[2] H. Zhou, F. Biglari, C. M. Davies, and K. Nikbin, "Simulating Residual Stress Profiles of Welds With Re-Heat Cracking in an Ex-Serviced AISI 316H Weld Header," in *ASME 2013 Pressure Vessels and Piping Conference*, 2013, pp. V06AT06A062–V06AT06A062.

[3] F. Vakili-Tahami and D. R. Hayhurst, "Failure of a welded pressure vessel due to creep: damage initiation, evolution and reheat cracking," *Philos. Mag.*, vol. 87, no. 28, pp. 4383–4419, Aug. 2007.

[4] B. Chen, P. E. J. Flewitt, D. J. Smith, and C. P. Jones, "An improved method to identify grain boundary creep cavitation in 316H austenitic stainless steel," *Ultramicroscopy*, vol. 111, no. 5, pp. 309–313, 2011.

[5] B. Chen, P. E. J. Flewitt, and D. J. Smith, "Microstructural sensitivity of 316H austenitic stainless steel: Residual stress relaxation and grain boundary fracture," *Mater. Sci. Eng. A*, vol. 527, no. 27–28, pp. 7387–7399, Oct. 2010.

[6] B. Chen, P. E. J. Flewitt, D. J. Smith, and C. M. Younes, "A Microstructural Sensitivity Study of 316H Austenitic Stainless Steel to Inter-granular Creep Fracture," in *Key Engineering Materials*, 2012, vol. 488, pp. 658–661.

[7] C. Maharaj, J. P. Dear, and A. Morris, "A Review of Methods to Estimate Creep Damage in Low-Alloy Steel Power Station Steam Pipes," *Strain*, vol. 45, no. 4, pp. 316–331, 2009.

[8] P. J. Holt, "Harlepool/Heysham I superheater Header Weld S4: Finite Element Modelling of Creep and Reheat Crack Initiation," 1996.

[9] P. J. Holt, "Heysham I/Hartlepool superheater Header Weld S4- Revised Finite Element Residual Stress and Reheat Cracking Analysis," 1997.

[10] R. P. Skelton, I. W. Goodall, G. A. Webster, and M. W. Spindler, "Factors affecting reheat cracking in the HAZ of austenitic steel weldments," *Int. J. Press. Vessel. Pip.*, vol. 80, no. 7–8, pp. 441–451, Jul. 2003.

[11] D. R. Hayhurst, F. Vakili-Tahami, and J. Q. Zhou, “Constitutive equations for time independent plasticity and creep of 316 stainless steel at 550 °C,” *Int. J. Press. Vessel. Pip.*, vol. 80, no. 2, pp. 97–109, Feb. 2003.

[12] H. Zhou, “A Simplified Fracture Mechanics and Continuum Damage Based Numerical Modelling Approach to Predict Long Term Creep Crack Growth in Components Containing Welds,” Imperial College London, 2015.

[13] D. Deng and H. Murakawa, “Numerical simulation of temperature field and residual stress in multi-pass welds in stainless steel pipe and comparison with experimental measurements,” *Comput. Mater. Sci.*, vol. 37, no. 3, pp. 269–277, Sep. 2006.

[14] D. J. Smith, P. J. Bouchard, and D. George, “Measurement and prediction of residual stresses in thick-section steel welds,” *J. Strain Anal. Eng. Des.*, vol. 35, no. 4, pp. 287–305, 2000.

[15] D. George, “Measurement of residual stress in thick section welds.” PhD thesis, University of Bristol, 2000.

[16] K. M. Nikbin, D. J. Smith, and G. A. Webster, “Prediction of Creep Crack Growth from Uniaxial Creep Data,” *Proc. R. Soc. London A Math. Phys. Eng. Sci.*, vol. 396, no. 1810, pp. 183–197, Nov. 1984.

[17] K. M. Nikbin, D. J. Smith, and G. A. Webster, “Influence of creep ductility and state of stress on creep crack growth,” *Adv. life Predict. methods Elev. Temp.*, pp. 249–258, 1983.

[18] K. M. Nikbin, D. J. Smith, and G. A. Webster, “An Engineering Approach to the Prediction of Creep Crack Growth,” *J. Eng. Mater. Technol.*, vol. 108, no. 2, pp. 186–191, Apr. 1986.

[19] Y. Sakanashi, S. Gungor, and P. J. Bouchard, “Measurement of Creep Deformation in Stainless Steel Welded Joints,” in *Optical Measurements, Modeling, and Metrology, Volume 5 SE - 45*, T. Proulx, Ed. Springer New York, 2011, pp. 371–378.

[20] I. W. Goodall and R. A. Ainsworth, “An Assessment Procedure for the High Temperature Response of Structures,” in *Creep in Structures SE - 35*, M. Życzkowski, Ed. Springer Berlin Heidelberg, 1991, pp. 303–311.

[21] A. Mehmanparast., C. M. Davies., D. W. Dean and K. Nikbin, *Effects of plastic pre-straining level on the creep deformation, crack initiation and growth behaviour of 316H stainless steel*. International journal of pressure vessels and piping, 141, pp.1-10. 2016.

[22] A. Mehmanparast, C. M. Davies, G. A. Webster, and K. M. Nikbin, “Creep crack growth rate predictions in 316H steel using stress dependent creep ductility,” *Mater. High Temp.*, vol. 31, no. 1, pp. 84–94, Jan. 2014.

[23] A. Mehmanparast, *Prediction of creep crack growth behaviour in 316H stainless steel for a range of specimen geometries*. International Journal of Pressure Vessels and Piping, 120, pp.55-65, 2014.

[24] H. Quintero and A. Mehmanparast, *Prediction of creep crack initiation behaviour in 316H stainless steel using stress dependent creep ductility*. International Journal of Solids and Structures, 97, pp.101-115, 2016.

[25] A. J. Perry, "Cavitation in creep," *J. Mater. Sci.*, vol. 9, no. 6, pp. 1016–1039, 1974.

[26] A. Mehmanparast, C. M. Davies, D. W. Dean, and K. M. Nikbin, "The influence of pre-compression on the creep deformation and failure behaviour of Type 316H stainless steel," *Eng. Fract. Mech.*, vol. 110, no. 0, pp. 52–67, Sep. 2013.

[27] S. Maleki., A. Mehmanparast and K. Nikbin, *Creep Crack Growth Prediction of Very Long Term P91 Steel Using Extrapolated Short-Term Uniaxial Creep Data*. In Pressure Vessels and Piping Conference (Vol. 55706, p. V06AT06A033). American Society of Mechanical Engineers, 2013.

[28] "ASTM E 1457-07e3:Standard test for measurement of creep crack growth times in metals," *ASTM Stand.*, vol. 3, no. 1, pp. 1–25, 2011.

[29] A. Mehmanparast., C. M. Davies., D. W. Dean and K. Nikbin, *Material pre-conditioning effects on the creep behaviour of 316H stainless steel*. International journal of pressure vessels and piping, 108, pp.88-93, 2013.

[30] C. M. Davies., D. W. Dean., A. Mehmanparast and K. Nikbin, *Compressive pre-strain effects on the creep and crack growth behaviour of 316H stainless steel*. In Pressure Vessels and Piping Conference (Vol. 49255, pp. 323-330), 2010.

[31] A. Mehmanparast., C. M. Davies., D. W. Dean and K. Nikbin, *The influence of cold pre-compression on high temperature deformation and fracture behaviour of 316H stainless steel*. In International Conference on Engineering Structural Integrity Assessment 24th-25th May, 2011.

[32] D. W. Dean and D. N. Gladwin, "Creep crack growth behaviour of Type 316H steels and proposed modifications to standard testing and analysis methods," *Int. J. Press. Vessel. Pip.*, vol. 84, no. 6, pp. 378–395, Jun. 2007.

[33] A. Bettison, "The Influence of Constraint on the Creep Crack Growth of 316H Stainless Steel," Imperial College London, 2001.